Porous Biomass Carbon Coated with SiO_2 as High Performance Electrodes for Capacitive Deionization

Guixiang Quan, Hui Wang, Fan Zhu, and Jinlong Yan*

The electrosorption capacity of an electrode strongly depends on the surface properties of the electrode material, such as the surface area, pore microstructure, and pore size distribution. Carbon-based electrode materials for capacitive deionization (CDI) or electrosorption processes suffer from problems with high manufacturing costs, poor electrical conductivity, and poor wettability. The thin-film coating of SiO_2 on porous biomass carbon may provide an alternative electrode material for double-layer applications. In this paper, the activated porous biomass carbon (AWSC) was first obtained through a simple potassium hydroxide (KOH) activation of wheat straw carbon (WSC) as the precursor, and then thin-film SiO_2 coated AWSC (SiO_2@AWSC) was prepared by a sol-gel coating process. Scanning electron microscope (SEM) imaging of SiO_2@AWSC demonstrated that a SiO_2 thin-film was deposited on the surface of AWSC without changing the opening structure. Compared to WSC, the Brunauer-Emmett-Teller (BET) surface area of SiO_2@AWSC was greatly increased, and presented obvious micropore and mesopore distributions. Further electrochemical analyses were performed *via* cyclic voltammetry, galvanostatic charge/discharge, and electrochemical impedance. The electrochemical results showed that SiO_2@AWSC electrodes showed increased electrosorption capacitance, which were attributed to a large specific surface area, a porous structure, and enhanced wettability.

Keywords: Biomass carbon; KOH activation; Capacitive deionization; SiO_2 thin-film; Electrosorption capacitance

*Contact information: School of Environmental Science and Engineering, Yancheng Institute of Technology, Yancheng 224051, China; *Corresponding Author: yjlyt4788@126.com*

INTRODUCTION

Due to the continuously rising population and the expanding chemical industry, a shortage of fresh water has become one of the most serious global problems (Subramani and Jacangelo 2015; Suss *et al.* 2015; Liu *et al.* 2017a). About 98% of the earth's water is seawater or brackish water, making seawater desalination a promising way to solve the water crisis. Such traditional desalination technologies as thermal separation and reverse osmosis are commonly used. However, these traditional methods are always energy and cost intensive (Yang *et al.* 2014; Liu *et al.* 2015a). As an alternative, capacitive deionization (CDI) has emerged as a promising water desalination technique that has drawn great attention. Operating with a low external power supply (less than 2 V), the CDI provided an energy-saving solution to obtain clean water without secondary pollution (Huang *et al.* 2017; Liu *et al*. 2017b).

As an electrochemical water treatment method, CDI is based on the mechanism of electric double layer (EDL) capacitors. Using an external electrostatic field, salt ions can

move to electrodes with an opposite charge and be adsorbed within the EDL that is formed between the salty solution and the electrode interface (Wang *et al*. 2016, 2017). Therefore, CDI performance is largely determined by the physical properties and internal structure of the electrode materials, such as specific surface area, pore structure, conductivity, and wettability (Porada *et al*. 2013). Until now, carbon-based materials, such as activated carbon (Liu *et al*. 2016), carbon nanotubes (Nie *et al*. 2012), carbon aerogel (Xu *et al*. 2008), and mesoporous carbon (Tsouris *et al*. 2011), are widely employed in CDI electrodes due to their high specific surface area, good conductivity, and chemical stability. However, CDI is still facing a major problem of the high cost of electrode materials.

Recently, biomass wastes have been considered for use as a potential raw material source for the preparation of porous carbons; these biomass wastes are comparatively cheap and abundant (Hou *et al*. 2014; Zhao *et al*. 2016). For instance, Kim *et al.* (2006) prepared bamboo-based carbons through carbonization and subsequent activation with steam, and the specific surface area values ranged from 445 m^2 g^{-1} to 1025 m^2 g^{-1}. Uçar *et al*. (2009) focused on pomegranate seeds derived from disordered carbonaceous materials with $ZnCl_2$ activation, and the activation conditions were deeply investigated. Until now, most reports concerning biomass-derived carbon have focused on the preparation methods. Nevertheless, the surface properties of carbon materials play a great role on the performance of experiments. For CDI electrodes, the surface polarity and wettability are very important. An electrode material with good wettability is beneficial for solution permeation into the inner pores, indicating efficient utilization of a specific surface (Jia and Zou 2012). Additionally, the surface polarity of electrode materials is related to the interactions between the electrode and ions (Liu *et al.* 2015b).

Herein, porous carbon derived from biomass and coated with nanoporous thin-films of SiO_2 was well prepared. The effects of silicon-coating conditions and carbonization on the texture, morphology, and specific surface area of the porous carbon were systematically studied. The electrochemical characteristics of the as-prepared porous carbon electrodes allowed for a greater understanding of the specific capacitance and inner resistance. A range of electrodes were employed to comprehensively compare the electrosorption performance.

EXPERIMENTAL

Materials

Tetramethy orthosilicate (TMOS) and tetrapropy orthosilicate (TPOS) were obtained from Aladdin (Aladdin Industrial Corporation, Shanghai, China) with a purity of 98%. The sodium chloride (NaCl) and hydrogen chloride (HCl) were obtained from Sinopharm Chemical Regent Company (Shanghai, China). Ammonium hydroxide was American Chemical Society (ACS) reagent grade. High-purity nitrogen was used to provide an oxygen-free environment. Double-distilled (DD) water was used in all of the experiments.

Preparation of wheat straw carbon (WSC)

Wheat straw carbon (WSC) was purchased from Sanli Company (Henan Province, China), which was produced by treating wheat straw at 350 °C to 550 °C under limited

oxygen supply. The WSC was then washed with ethyl alcohol and water, dried at 100 °C, and then sieved with 100-mesh (0.15 mm). The sieved WSC was first impregnated by adding it to 3.0 M KOH at 1:1 of the mass ratio of KOH/WSC for 24 h in 250-mL beakers, then filtrated and dried at 105 °C for 24 h. After being dried at 105 °C, the mixture was placed in a tube furnace and heated at the activation temperature of 800 °C under a N_2 atmosphere for 2 h. After cooling to room temperature, the mixtures were thoroughly washed with 0.1 M HCl and hot DD water until the pH was neutral. Then, the obtained activated WSC (AWSC) was dried at 105 °C overnight and kept in a desiccator for further use.

Coating of AWSC with SiO_2

The silica sols were synthesized with methods described by Chu *et al.* (1997). The basic SiO_2 sol was prepared by adding ammonium hydroxide (0.5 M) to the TMOS or TPOS. Then, the colloidal suspension was put into dialysis tubing and dialyzed with distilled water to remove ammonia and ethanol until the pH was near 8.5. Then 1.5 g AWSC was added into the basic SiO_2 sol and stirred until well-blended, and the ratio of AWSC/SiO_2 ranges from 0.5-3.0. The above slurry was oven-dried at 80 °C and then heated in a tube furnace up to 800 °C for 120 min with the rising rate of 2 ^oC/min under nitrogen protection. Finally, it was washed with HCl and ionized water until the pH was 7.0. The AWSC coated with SiO_2 produced from TMOS was named M-SiO_2@AWSC, while from TPOS it was named P-SiO_2@AWSC.

Methods

Sample Characterization

A scanning electron microscope (SEM) (S-520, Hitachi Co., Tokyo, Japan) was used to analyze the surface morphology of silica sols-coated carbon. The pore size distribution, Brunauer-Emmett-Teller (BET) surface area, and pore volume were determined by N_2 adsorption/desorption isotherms at 77 K. Prior to nitrogen adsorption experimentation to determine surface properties, all samples were degassed at 573 K under vacuum for 4 h. The specific surface area was calculated according to the BET equation using relative pressures in the data range between 0.06 and 0.2. The pore size distribution was determined *via* Barret–Joyner–Halenda method (BJH) model. The x-ray diffraction (XRD) measurements were recorded on a Siemens D500 diffractometer (Siemens AG, Munich, Germany) with a graphite monochromator and Cu Kα radiation.

Electrochemical performances of SiO_2@AWSC electrodes

The electrodes were fabricated by placing the mixture of SiO_2@AWSC, polytetrafluoroethylene (PTFE), and ethanol onto graphite sheets and then drying them at 105 °C overnight. The ratio of SiO_2@AWSC, PTFE was 9:1. The electrochemical performance of SiO_2@AWSC electrodes was measured by cyclic voltammetry. The cyclic voltammetry (CV) was performed using an electrochemical workstation (CS-350, Wuhan CorrTest Instruments Corp., Ltd., Wuhan, China) with three-electrode cells. The SiO_2@AWSC electrode, graphite electrode, and Ag/AgCl electrode were used as the working electrode, counter electrode, and reference electrode, respectively. The cyclic voltammetry was performed with a scanning rate of 10 mV s^{-1}, the potential range was from -0.5 V to 0.5 V, and the electrolyte solution was 0.5 M NaCl.

The specific capacitance (F g^{-1}) can be obtained from the CV test according to the following equation,

$$C_m = \frac{\int i \, dV}{2v\Delta V m} \quad (1)$$

where C_m is the specific capacitance (F g^{-1}), i is the response current density (A), v is the sweep rate (V/s) , ΔV is the potential window and m is the mass of the porous carbon (g).

RESULTS AND DISCUSSION

Morphology and Structure of Samples

The SEM images of WSC, AWSC, M-SiO_2@AWSC, and P-SiO_2@AWSC are shown in Fig. 1.

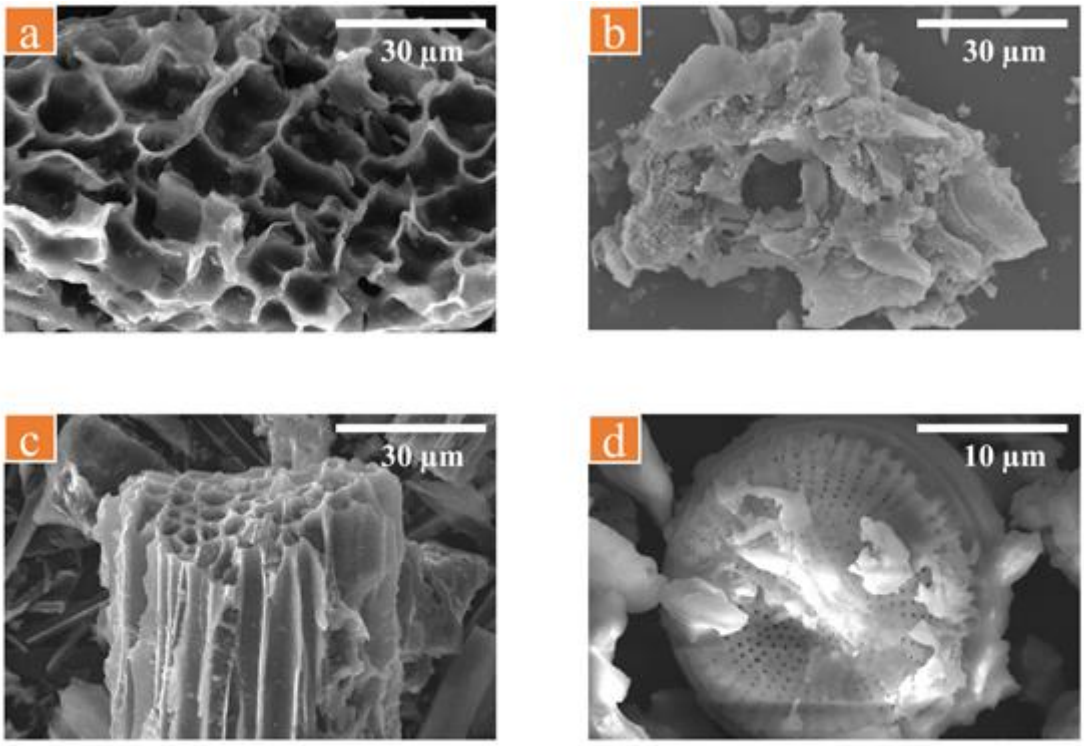

Fig. 1. SEM images of WSC (a), AWSC (b), M-SiO_2@AWSC (c), and P-SiO_2@AWSC (d)

As shown in Fig. 1a, the WSC exhibited several porous channels due to the tissue structure of wheat straw. The ports of the porous channels were open, which is beneficial for mass transportation. In Fig. 1b, the AWSC shows a porous structure with a rough surface with a particle size of approximately 10 μm after activation, indicating that the structure of WSC was destroyed and many defects were introduced on the surface of the WSC. During the activation process, the K^+ ions reacted with the carbon atom on the WSC surface, so the pores were formed *in situ*. After SiO_2 film coating, the morphology of M-SiO_2@AWSC and P-SiO_2@AWSC were hardly changed, which indicated that the opening

structure can be preserved, as shown in Fig. 1c and 1d. It should be noted that the M-SiO_2@AWSC and P-SiO_2@AWSC showed rough surfaces as compared with WSC, because the SiO_2 film was effectively coated on the surface *via* sol-gel methods. Furthermore, the SiO_2 films on the surface M-SiO_2@AWSC were smoother and finer than that of P-SiO_2@AWSC, because the smaller size particles were formed using TMOS as the silicon source. During the hydrolysis process, TMOS will react with water faster and result in a higher concentration of hydrolyzed species due to the smaller alkyl groups, while TPOS with its larger alkyl groups reacts slower, which led to larger particle sizes (Chu *et al.* 1997).

To further investigate the distribution of elements on the surface of M-SiO2@AWSC, the EDS mappings are provided in Fig. 2.

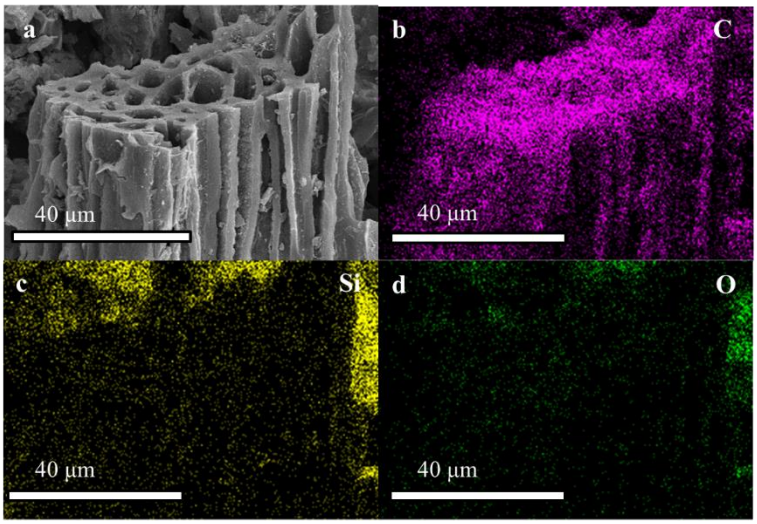

Fig. 2. (a) SEM image of M-SiO_2@AWSC, (b-c) the EDS mapping image of C, Si and O elements

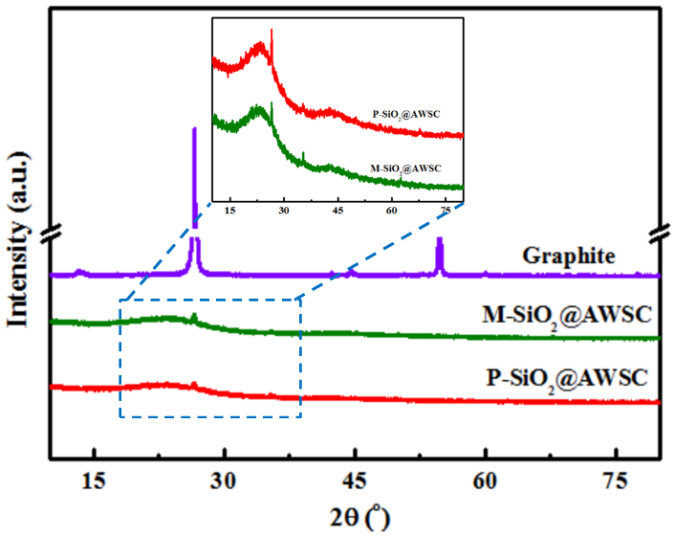

Fig. 3. XRD patterns of graphite, M-SiO_2@AWSC and P-SiO_2@AWSC and graphite

The C, Si, and O were dominant in the M-SiO_2@AWSC. Clearly, the Si element was evenly distributed on the surface of carbon according to the EDS mapping images, indicating SiO_2 film had been successfully coated on the surface of AWSC. The result of EDS mapping further demonstrated that the sol-gel methods is an effective way of coating the M-SiO_2 on the surface of carbon materials.

Figure 3 shows the XRD patterns of the M-SiO_2@AWSC and P-SiO_2@AWSC and graphite. Both of M-SiO_2@AWSC and P-SiO_2@AWSC showed two broad diffraction peaks at approximately 2θ = 23.4º and 43.0º, which are indexed as (002) and (100) in the pseudographitic domains (Ding *et al.* 2015). As compared to standard graphite diffraction peaks, the (002) and (100) peaks of M-SiO_2@AWSC and P-SiO_2@AWSC were broader, indicating the amorphous structure of these two samples (Wu *et al.* 2015). Moreover, M-SiO_2@AWSC and P-SiO_2@AWSC also have sharp peaks at approximately 2θ = 26.5º, which can be ascribed to the characteristic peak of SiO_2. Therefore, it can be concluded that the SiO_2 films were introduced into the carbon structure through the silicon source hydrolysis.

The N_2 sorption is always used to analyze the pore structure and the specific surface area of materials. Figure 4 shows the N_2 adsorption-desorption isotherms of the WSC, M-SiO_2@AWSC, and P-SiO_2@AWSC. The WSC showed a type I isotherm, which indicated that micropores were determinate in WSC. The M-SiO_2@AWSC and P-SiO_2@AWSC exhibited type IV isotherms with an obvious H4 hysteresis loop at P_0/P = 0.4 to 1.0, suggesting that abundant mesopores are present in M-SiO_2@AWSC and P-SiO_2@AWSC (Sun *et al*. 2013).

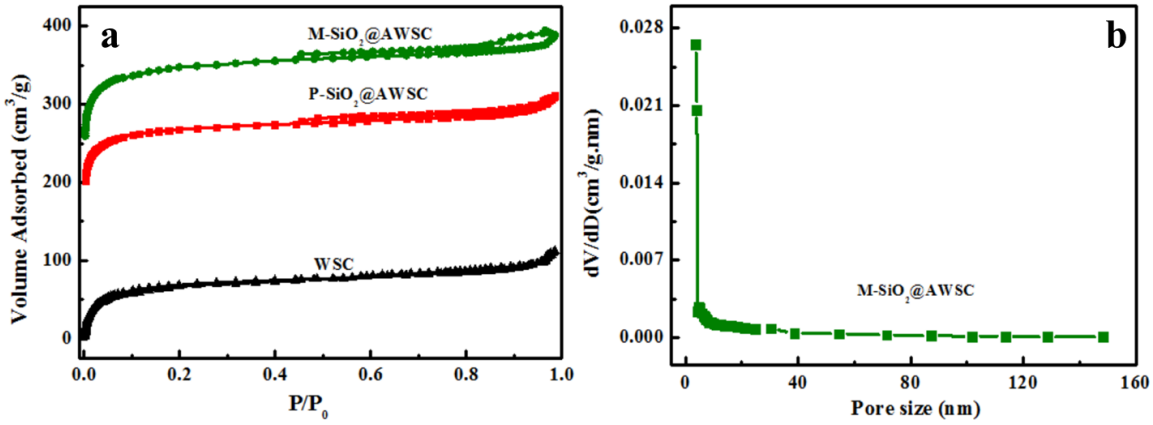

Fig. 4. (a) N_2 sorption isotherms of WSC, M-SiO_2@AWSC, and P-SiO_2@AWSC, (b) pore size distribution of M-SiO_2@AWSC

As calculated, the BET surface areas of the WSC, M-SiO_2@AWSC, and P-SiO_2@AWSC were 7.53 m^2 g^{-1}, 1206.21 m^2 g^{-1}, and 925.11 m^2 g^{-1}, respectively. The specific surface areas of M-SiO_2@AWSC and P-SiO_2@AWSC rose massively after the SiO_2 coating, because numbers of mesopores were well introduced into the carbon structure. The M-SiO_2@AWSC showed a much higher specific surface area than P-SiO_2@AWSC, which resulted from the SiO_2 with a smaller partial size coating the surface of WSC. With smaller alkyl groups, the TMOS reacted with water faster and led to a smaller pore size. As can be seen from pore size distribution curve of M-SiO_2@AWSC in

Fig. 4b, the pore size was mostly centered around 3.8 nm, further indicating the mesoporous structure of M-SiO_2@AWSC. Moreover, the effect of TMOS amount on specific surface area of the M-SiO_2@AWSC was investigated in detail. According to the measurement results, with smaller ratio of TMOS/AWSC, the specific surface area (645 m^2 g^{-1}) was much less than 1206 m^2 g^{-1} due to the insufficient coating of M-SiO_2. However, when the ratio of TMOS/AWSC is increased to 3.0, the specific surface area decreased to 582 m^2 g^{-1}, because excessive hydrolysis of TMOS blocks some pores of AWSC. The higher specific surface area of M-SiO_2@AWSC likely provided more adsorption sites for ion adsorption and the mesoporous structure accelerated fast ion transportation. Thus, the M-SiO_2@AWSC shows great potential in CDI application.

Electrochemical Performance

To investigate the electrochemical performance of M-SiO_2@AWSC and P-SiO_2@AWSC, the CV test was conducted in a 1 M NaCl solution with a scan rate of 10 mV s^{-1}; the CV curves are shown in Fig. 5. When the electric potential increased, the current increased accordingly, indicating that the electrodes had fast responses to electrical potential increase. Once the potential decreased, the current also decreased, which indicated that the electrosorption process was reversible. There were no obvious redox peaks in the CV curves, suggesting that the ions adsorbed on the electrode surface by forming an electric double layer due to coulombic interaction rather than an electrochemical reaction (Peng *et al.* 2012). As calculated according to Eq. 1, the specific capacitances of M-SiO_2@AWSC and P-SiO_2@AWSC were 156.8 F g^{-1} and 136.2 F g^{-1}. The higher specific capacitance of M-SiO_2@AWSC resulted from the larger specific surface area, which provided more adsorption sites. Besides, as can be seen from the inset, the contact angle of M-SiO_2@AWSC electrode was about 40°, indicating the good hydrophily of the electrode. Hence, with porous structure and hydrophilic surface, the M-SiO_2@AWSC electrode exhibited higher capacitance.

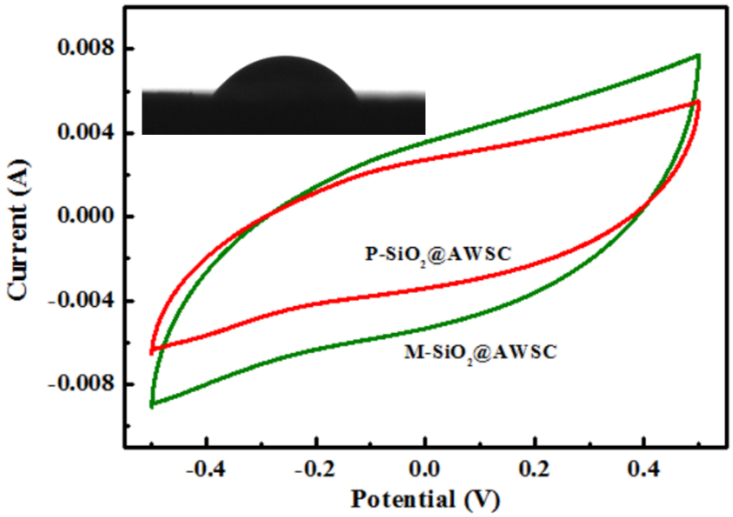

Fig. 5. CV curves of M-SiO_2@AWSC and P-SiO_2@AWSC in a 0.5 M NaCl solution. The inset is the contact angle optical image of M-SiO_2@AWSC electrode.

To further understand the electrosorption mechanism of M-SiO_2@AWSC, the influence of the TMOS/WSC ratio on the electrochemical performance of the M-SiO_2@AWSC was investigated. As shown in Fig. 6a, when the mass ratio of TMOS/WSC increased from 0.5 to 3.0, the specific capacitance of the M-SiO_2@AWSC electrodes increased at first, and then decreased. When the ratio reached 2.0, the specific capacitance reached a maximum. As calculated, specific capacitance of TMOS-2.0 was 156.8 F g^{-1}, while that of TMOS-0.5, TMOS-1.0, and TMOS-3.0 were 75.8 F g^{-1}, 116.8 F g^{-1}, and 138.4 F g^{-1}, respectively. With a low TMOS/AWSC ratio, the SiO_2 film could not be well established, which led to a lower specific surface area and fewer transportation channels for salt ions to undergo adsorption and diffusion. However, when the TMOS/AWSC ratio was too high, the excessive TMOS sol would block the pore structure of AWSC, which led to a lower specific capacitance. It could be concluded that a suitable TMOS/AWSC ratio was important to the formation of M-SiO_2@AWSC with a higher surface area and richer pore structure.

Figure 6b shows the effect of scanning rate on the electrochemical properties of M-SiO_2@AWSC. With lower scanning rates (5 mV s^{-1} or 10 mV s^{-1}), the CV curves kept a rectangular shape, which indicated that the M-SiO_2@AWSC electrodes exhibited ideal capacitive behavior. However, when the scan rate was increased to 20 mV s^{-1}, the profile was distorted and turned into a leaf-like shape; the specific capacitance decreased accordingly. With a lower scan rate, salt ions have enough time to migrate into the inner pores of electrodes, and then an electric double layer can form completely. Thus, a better capacitive behavior is obtained. Nevertheless, with higher scanning rates, ions barely have time to penetrate into the deeper pores of the electrodes, which leads to a reduced accessible surface area for ion adsorption, and thus results in a decreased specific capacitance (Wen *et al.* 2013). Therefore, a lower scanning rate was beneficial for better electric double layer capacitive behavior.

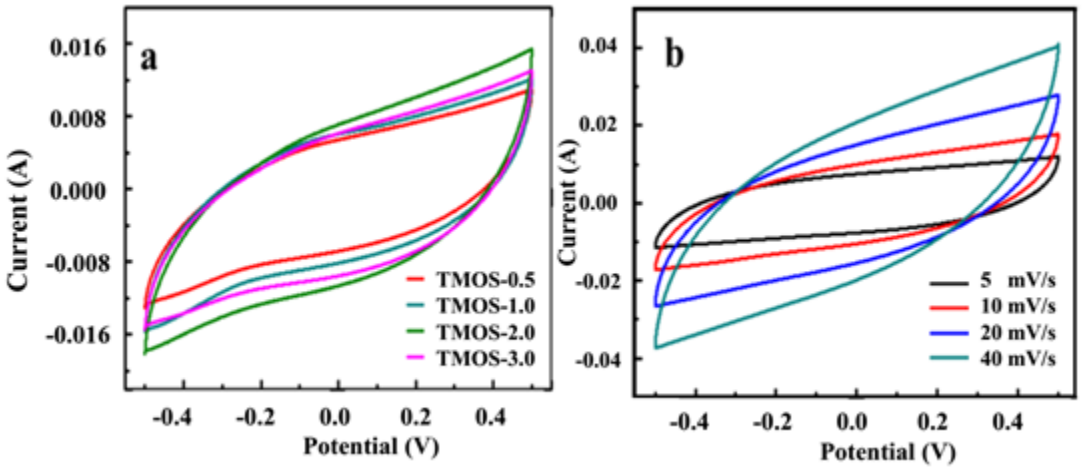

Fig. 6. CV curves of M-SiO_2@AWSC electrodes with different TMOS/WSC ratios (a) and at different scan rates (b)

To further investigate the electrosorption performance of M-SiO_2@AWSC electrodes, galvanostatic charge-discharge measurements were conducted at various current densities, from 0.2 to 1.0 A g^{-1} with a potential window of -0.5 V to 0.5 V, and the

results are shown in Fig. 7. The galvanostatic charge-discharge curves of the M-SiO_2@AWSC electrode kept a triangular shape at each current density, which indicated excellent reversibility of the M-SiO_2@AWSC electrode, and thus revealed that the ions adsorbed on the electrode surface were due to the electric double layer formation rather than due to an electrochemical reaction. The sudden voltage drop appears at the beginning of the discharge processes, which is the iR drop. At a low current, the iR drop was negligible, which indicated that the M-SiO_2@AWSC electrode had a low inner resistance. With increasing current density, the iR drop also increased due to incomplete discharge at the high current density (Wang *et al.* 2014). The discharge time decreased with increasing current density, because salt ion diffusion was impeded.

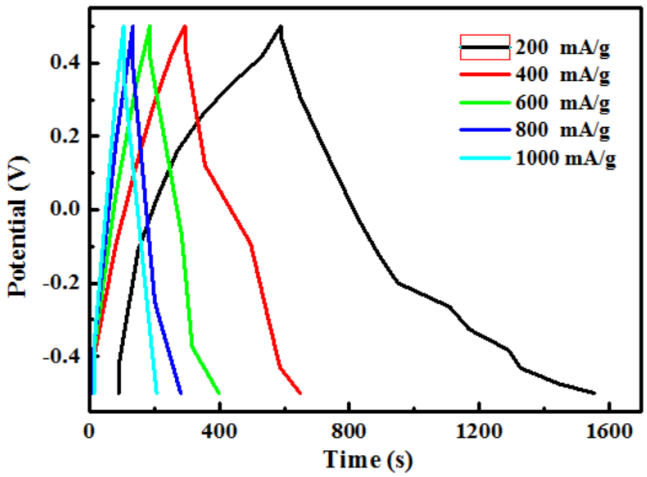

Fig. 7. Galvanostatic charge-discharge curves of M-SiO_2@AWSC electrodes at different current densities

A batch mode CDI experiment was conducted to determine the electrosorption performance of WSC, AWSC, M-SiO_2@AWSC, and P-SiO_2@AWSC electrodes (Fig. 8a). As shown in Fig. 6b, the solution conductivity sharply decreased once voltage was applied, and then the adsorption reached an equilibrium value after approximately 45 min. The electrodes had enough time for salt ion adsorption at the initial stage of electrosorption, so the solution conductivity decreased rapidly. As the experiment proceeded, the accessible surface area of the electrodes decreased continuously, resulting in a gradually-decreasing trend (Wang *et al.* 2014). Importantly, the solution conductivity with M-SiO_2@AWSC electrodes decreased more rapidly than with WSC, AWSC, and P-SiO_2@AWSC, indicating that the M-SiO_2@AWSC can adsorb more salt ions. For the NaCl solution with an initial conductivity of 60 μs cm^{-1}, the conductivity decreased to 10.2 μs cm^{-1} using M-SiO_2@AWSC electrodes for 30 min, to a lower value than that of WSC (48.2 μs cm^{-1}), AWSC (29.6 μs cm^{-1}), and P-SiO_2@AWSC (15.2 μs cm^{-1}) (Fig. 8b). As calculated, the electrosorption capacity of M-SiO_2@AWSC electrodes was 2.67 mg g^{-1}, which is higher than that of WSC, AWSC, P-SiO_2@AWSC and some recent reported electrode materials (Table 1). The enhanced electrosorption capacity of M-SiO_2@AWSC was ascribed to the following causes. First, the M-SiO_2@AWSC had a much larger surface area than that of the WSC and P-SiO_2@AWSC, which can provide more adsorption sites for salt ions. Secondly, the small SiO_2 particles were uniformly distributed on the surface of M-

SiO_2@AWSC, resulting in improved wettability. The aqueous solution can more easily permeate into the M-SiO_2@AWSC electrode, so the inner pores and surface area of the electrode can be further used. Therefore, the M-SiO_2@AWSC with larger specific surface area and more uniform SiO_2 coating showed better performance in the electrosorption area. The electrosorption–desorption cycles were conducted to further examine the regeneration capacities of the obtained electrodes. The adsorbed ions can effectively revert to the bulk solution when the external potential is removed, so the electrode can be regenerated for further use without any secondary waste (Fig. 8b).

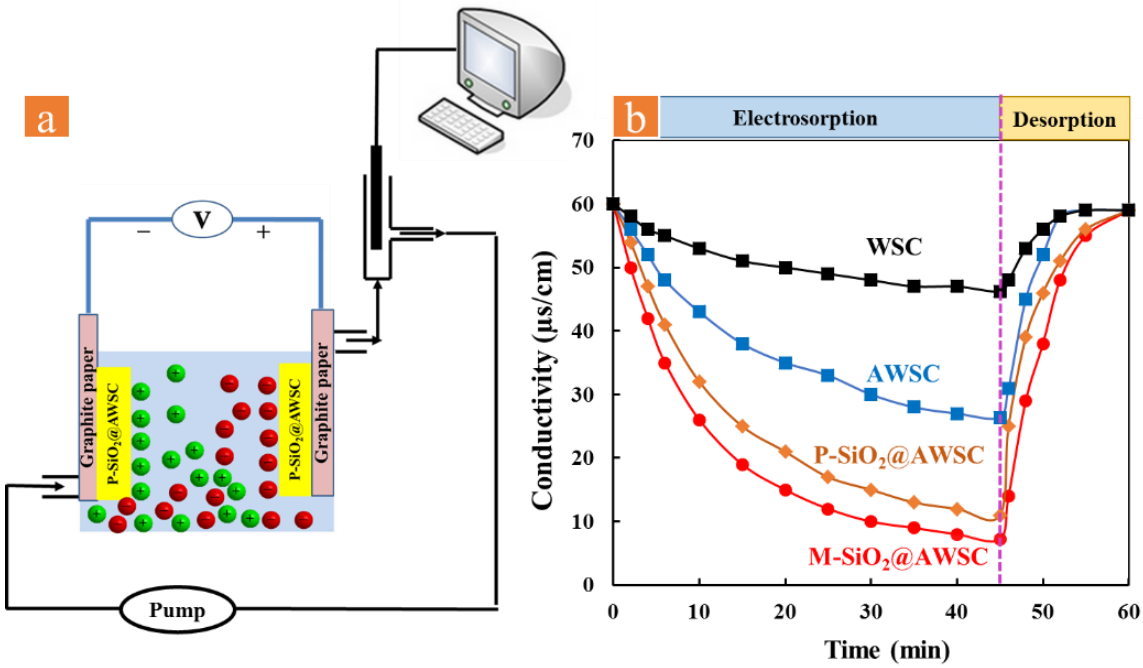

Fig. 8. Schematic illustration of CDI process (a) and conductivity changes *vs.* deionization time curves (b)

Table 1. Comparison of Electrosorption Capacity among Different Electrode Materials

Electrodes	Solution concentration (mg/L)	Electrosorption capacity (mg/g)	References
graphene	~30	1.36	Li *et al.* 2010
ACF -CNT	~60	1.3	Wang *et al.* 2010
Woven carbon fiber	-	1.87	Ryoo and Seo 2003
Mesoporous carbon	~25	0.69	Zou *et al.* 2008
AC	~25	0.25	Zou *et al.* 2008

CONCLUSIONS

Porous carbon derived from waste biomass with a SiO_2 nanoparticle coating was prepared for experimentation. The influence of coating conditions, especially of the silicon source on the structure and surface properties of porous carbon, were investigated in detail.

1. When TMOS was used as the silicon source, the smaller SiO_2 nanoparticles were uniformly coated on the surface of porous carbon. The obtained M-SiO_2@AWSC exhibited improved specific surface area and good wettability by aqueous solutions.
2. The electrochemical measurements in 0.5 M NaCl solution revealed that the M-SiO_2@AWSC electrodes showed high specific capacitance and low inner resistance. In further electrosorption tests, the electrosorption of M-SiO_2@AWSC electrodes was 2.67 mg g^{-1}, much higher that of P-SiO_2@AWSC and WSC. These promising results revealed that the effective surface modification of carbon materials is suitable for high-performance electrosorption.

ACKNOWLEDGMENTS

The authors gratefully acknowledge financial support from the National Natural Science Foundation of China (Grant No. 21677119) and the Natural Science Foundation for Colleges and Universities in Jiangsu Province (Grant No. 15KJB610015).

REFERENCES CITED

Chu, L., Tejedor-Tejedor, M. A. and Anderson, M. A. (1997). "Particulate sol-gel route for microporous silica gels," *Microporous Materials* 8(5-6), 207-213. DOI: 10.1016/S0927-6513(96)00068-5

Ding, J., Wang, H., Li, Z., Cui, K., Karpuzov, D., Tan, X., Kohandehghan, A., and Mitlin, D. (2015). "Peanut shell hybrid sodium ion capacitor with extreme energy–power rivals lithium ion capacitors," *Energy & Environmental Science* 8(3), 941-955. DOI: 10.1039/C4EE02986K

Hou, J., Cao, C., Ma, X., Idrees, F., Xu, B., Hao, X., and Lin, W. (2014). "From rice bran to high energy density supercapacitors: A new route to control the porous structure of 3D carbon," *Scientific Reports* 4, 7260. DOI: 10.1038/srep07260

Huang, Z. H., Yang, Z., Kang, F., and Inagaki, M. (2017). "Carbon electrodes for capacitive deionization," *Journal of Materials Chemistry A* 5(2), 470-496. DOI: 10.1039/C6TA06733F

Jia, B., and Zou, L. (2012). "Wettability and its influence on graphene nanosheets as electrode material for capacitive deionization," *Chemical Physics Letters* 548, 23-28. DOI: 10.1016/j.cplett.2012.06.016

Kim, C., Lee, J. W., Kim, J. H., and Yang, K. S. (2006). "Feasibility of bamboo-based activated carbons for an electrochemical supercapacitor electrode," *Korean Journal of Chemical Engineering* 23(4), 592-594. DOI: 10.1007/BF02706799

Li, H. B., Zou, L. D., Pan, L. K., and Sun, Z. (2010). "Novel graphene-like electrodes for

capacitive deionization," *Environmental Science & Technology* 44 (22), 8692-8697. DOI: 10.1021/es101888j

Liu, P. I., Chung, L. C., Ho, C. H., Shao, H., Liang, T. M., Chang, M. C., Ma, C. C. M., and Horng, R. Y. (2016). "Comparative insight into the capacitive deionization behavior of the activated carbon electrodes by two electrochemical techniques," *Desalination* 379, 34-41. DOI: 10.1016/j.desal.2015.10.008

Liu, L., Guo, X., Tallon, R., Huang, X., and Chen, J. (2017a). "Highly porous N-doped graphene nanosheets for rapid removal of heavy metals from water by capacitive deionization," *Chemical Communications* 53(5), 881-884. DOI: 10.1039/C6CC08515F

Liu, J., Lu, M., Yang, J., Cheng, J., and Cai, W. (2015a). "Capacitive desalination of ZnO/activated carbon asymmetric capacitor and mechanism analysis," *Electrochimica Acta* 151, 312-318. DOI: 10.1016/j.electacta.2014.11.023

Liu, Y., Nie, C., Liu, X., Xu, X., Sun, Z., and Pan, L. (2015b). "Review on carbon-based composite materials for capacitive deionization," *RSC Advances* 5(20), 15205-15225. DOI: 10.1039/C4RA14447C

Liu, P., Yan, T., Shi, L., Park, H. S., Chen, X., Zhao, Z. G. and Zhang, D. S. (2017b). "Graphene-based materials for capacitive deionization," *Journal of Materials Chemistry A* 5(27), 13907-13943. DOI: 10.1039/C7TA02653F

Nie, C. Y., Pan, L. K., Li, H. B., Chen, T. Q., Lu, T., and Sun, Z. (2012). "Electrophoretic deposition of carbon nanotubes film electrodes for capacitive deionization," *Journal of Electroanalytical Chemistry* 666, 85-88. DOI: 10.1016/j.jelechem.2011.12.006

Peng, Z., Zhang, D. S., Shi, L., and Yan, T. (2012). "High performance ordered mesoporous carbon/carbon nanotube composite electrodes for capacitive deionization," *Journal of Material Chemistry* 22(14), 6603-6612. DOI: 10.1039/C2JM16735B

Porada, S., Zhao, R., Van der Wal, A., Presser, V., and Biesheuvel, P. M. (2013). "Review on the science and technology of water desalination by capacitive deionization," *Progress in Materials Science* 58(8), 1388-1442. DOI: 10.1016/j.pmatsci.2013.03.005

Ryoo, M. W., and Seo, G. (2003). "Improvement in capacitive deionization function of activated carbon cloth by titania modification," *Water Research* 37(7), 1527-1534. DOI: 10.1016/S0043-1354(02)00531-6.

Subramani, A., and Jacangelo, J. G. (2015). "Emerging desalination technologies for water treatment: A critical review," *Water Research* 75, 164-187. DOI: 10.1016/j.watres.2015.02.032

Sun, L., Tian, C. G., Li, M. T., Meng, X. Y., Wang, L., Wang, R. H., Yin, J., and Fu, H. G. (2013). "From coconut shell to porous graphene-like nanosheets for high-power supercapacitors," *Journal of Materials Chemistry A* 1(21), 6462-6470. DOI: 10.1039/C3TA10897J

Suss, M. E., Porada, S., Sun, X., Biesheuvel, P. M., Yoon, J., and Presser, V. (2015). "Water desalination *via* capacitive deionization: What is it and what can we expect from it?," *Energy & Environmental Science* 8(8), 2296-2319. DOI: 10.1039/C5EE00519A

Tsouris, C., Mayes, R., Kiggans, J., Sharma, K., Yiacoumi, S., DePaoli, D., and Dai, S. (2011). "Mesoporous carbon for capacitive deionization of saline water,"

Environmental Science & Technology 45(23), 10243-10249. DOI: 10.1021/es201551e

Uçar, S., Erdem, M., Tay, T., and Karagöz, S. (2009). "Preparation and characterization of activated carbon produced from pomegranate seeds by $ZnCl_2$ activation," *Applied Surface Science* 255(21), 8890-8896. DOI: 10.1016/j.apsusc.2009.06.080

Wang, H., Shi, L., Yan, T. T., Zhang, J. P., Zhong, Q. D., and Zhang, D. S. (2014). "Design of graphene-coated hollow mesoporous carbon spheres as high performance electrodes for capacitive deionization," *Journal of Materials Chemistry A* 2(13), 4739-4750. DOI: 10.1039/C3TA15152B

Wang, M., Huang, Z. H., Wang, L., Wang, M. X., Kang, F. Y., and Hou, H. Q. (2010). "Electrospun ultrafine carbon fiber webs for electrochemical capacitive desalination," *New Journal of Chemistry* 34 (9), 1843-1845. DOI: 10.1039/c0nj00407c.

Wang, Z., Yan, T. T., Fang, J. H., Shi, L., and Zhang, D. S. (2016). "Nitrogen-doped porous carbon derived from a bimetallic metal-organic framework as highly efficient electrodes for flow-through deionization capacitors," *Journal of Materials Chemistry A* 4(28), 10858-10868. DOI: 10.1039/C6TA02420C

Wang, H., Yan, T. T., Shi, L., Chen, G., Zhang, J. P., and Zhang, D. S. (2017). "Creating nitrogen-doped hollow multiyolk@shell carbon as high performance electrodes for flow-through deionization capacitors," *ACS Sustainable Chemistry & Engineering* 5(4), 3329-3338. DOI: 10.1021/acssuschemeng.5b01113

Wen, X., Zhang, D. S., Yan, T. T., Zhang, J. P., and Shi, L. (2013). "Three-dimensional graphene-based hierarchically porous carbon composites prepared by a dual-template strategy for capacitive deionization," *Journal of Materials Chemistry A* 1(39), 12334-12344. DOI: 10.1039/C3TA12683H

Wu, X. L., Jiang, L., Long, C., and Fan, Z. J. (2015). "From flour to honeycomb-like carbon foam: Carbon makes room for high energy density supercapacitors," *Nano Energy* 13, 527-536. DOI: 10.1016/j.nanoen.2015.03.013

Xu, P., Drewes, J. E., Heil, D., and Wang, G. (2008). "Treatment of brackish produced water using carbon aerogel-based capacitive deionization technology," *Water Research* 42(10-11), 2605-2617. DOI: 10.1016/j.watres.2008.01.011

Yang, Z. Y., Jin, L. J., Lu, G. Q., Xiao, Q. Q., Zhang, Y. X., Jing, L., Zhang, X. X., Yan, Y. M., and Sun, K. N. (2014). "Sponge-templated preparation of high surface area graphene with ultrahigh capacitive deionization performance," *Advanced Functional Materials* 24(25), 3917-3925. DOI: 10.1002/adfm.201304091

Zhao, S. S., Yan, T. T., Wang, H., Zhang, J. P., Shi, L., and Zhang, D. S. (2016). "Creating 3D hierarchical carbon architectures with micro-, meso-, and macropores *via* a simple self-blowing strategy for a flow-through deionization capacitor," *ACS Applied Materials & Interfaces* 8(28), 18027-18035. DOI: 10.1021/acsami.6b03704

Zou, L. D., Li, L. X., Song, H. H, and Morris, G. (2008). "Using mesoporous carbon electrodes for brackish water desalination," *Water Research* 42(8), 2340-2348. DOI: 10.1016/j.watres.2007.12.022

Article submitted: August 30, 2017; Peer review completed: October 22, 2017; Revised version received and accepted: November 13, 2017; Published: November 22, 2017.
DOI: 10.15376/biores.13.1.437-449